Stokes flow due to point torques and sources in a spherical geometry

Alexander Chamolly* and Eric Lauga†
Department of Applied Mathematics and Theoretical Physics, University of Cambridge, Wilberforce Road, CB3 0WA, Cambridge, United Kingdom

(Received 15 April 2020; accepted 9 July 2020; published 27 July 2020)

Solutions to the Stokes equations written in terms of a small number of hydrodynamic image singularities have been a useful tool in theoretical and numerical computations for nearly 50 years. In this article, we extend the catalog of known solutions by deriving the flow expressions due to a general point torque and point source in the presence of a stationary sphere with either a no-slip or a stress-free (no-shear) boundary condition. For an axisymmetric point torque and a no-slip sphere the image system simplifies to a single image point torque, reminiscent of the solution for a point charge outside an equipotential sphere in electrostatics. By symmetry, this also gives a simple representation of the solution due to an axisymmetric point torque inside a rigid spherical shell. In all remaining cases, the solution can be described by a collection of physically intuitive point and line singularities. Our results will be useful for the theoretical modeling of the propulsion of microswimmers and efficient numerical implementation of far-field hydrodynamic interactions in this geometry.

DOI: 10.1103/PhysRevFluids.5.074202

I. INTRODUCTION

Since George Gabriel Stokes first wrote down the low-Reynolds number flow equations that now bear his name [1], countless studies have been devoted to their mathematical properties and applications in fluid mechanics [2–6]. Perhaps most fundamentally, their Green's function, corresponding to the flow due to a point force in an unbounded fluid, has been known since 1896 [7]. It is today referred to as the Stokeslet and has been applied and generalized in many different ways [3,4].

One such extension is achieved through adding several canceling point forces and taking the limit of zero separation in such a fashion that the product of their separation and their relative strengths remains finite. This process gives rise to higher-order faster decaying singularities such as force dipoles and quadrupoles, similar to charges in electrostatics but with an additional degree of complexity due to the vectorial nature of the Stokeslet. In particular, the force dipole singularity may be decomposed [8] into (i) a symmetric part, termed the stresslet, that corresponds to a symmetric hydrodynamic stress applied locally to the fluid, and (ii) an antisymmetric part, termed the rotlet, corresponding to a local hydrodynamic torque. These singularities also emerge naturally in the far-field asymptotic expansion of moving bodies in Stokes flow [3], and are useful for the modeling of suspensions of passive [6] and active [9,10] particles and cells swimming in fluids [11–17]. Furthermore, these singularities form the basis of boundary integral methods that are among the most powerful computational tools for Stokes flows [18].

*ajc297@cam.ac.uk
†e.lauga@damtp.cam.ac.uk

A different but desirable extension of the free-space Green's function adapts it to more complex geometries. In a landmark paper, Blake derived the singularity solution for a Stokeslet in the presence of a plane rigid wall [19] and later extended it to higher-order singularities [20]. Since then, these have been applied extensively for their relevance in computational fluid mechanics [18,21] and in the study of microorganisms near boundaries [22]. In a similar fashion, many other geometries have been explored, including fluid-fluid interfaces [23], the fluid outside [2,24] and inside a rigid sphere [25–27], and viscous fluid confined between parallel plates [28,29]. A concise account of the most important results and their derivations may be found in the textbook by Kim and Karrila [4]. More recently, a significant interest in regularized flow singularities and the corresponding image systems has also emerged [30–32], well suited, e.g., for the efficient numerical simulation of slender fibers in viscous fluid [33].

Given a set of well-posed boundary conditions, the solution to the Stokes equations is unique [4]. However, in many cases multiple equivalent formulations exist of the same solution, each with their own advantages and disadvantages. For problems in a spherical geometry, Lamb's general solution [34] is a useful mathematical tool since it provides a complete set of eigenfunctions, however it is often cumbersome to use in numerical applications and lacks physical intuition. A similar problem arises for multipole expansions about the center of the sphere, which are accurate for flows caused by disturbances far from the sphere, but become unwieldy when singularities near the sphere surface are considered [4]. A third option is given by Oseen's original solution [2], which is written as the free-space Stokeslet singularity plus an integral over the sphere surface that corrects for the no-slip boundary condition. Perhaps the most elegant and useful formulation, and motivated by the method of images, is written in terms of a distribution of hydrodynamic singularities. This form provides an intuitive physical interpretation, and since, unlike a multipole expansion, only singularities up to a finite order need to be calculated it is easy to achieve high numerical accuracy. Blake's solution for the Stokeslet near a wall is of this form, as are expressions for the Stokeslet near a spherical drop of arbitrary viscosity [35,36].

Most of the results in the literature concerning the singularity representation were derived in work that focused on the dynamics of passive suspensions, and thus limited to only the kind of singularities appearing at leading order there. In contrast, for problems such as the rotation of flagellar filaments outside bacterial cell bodies [37], or the growth of bubbles near catalytic colloids [38], it is necessary to obtain the solution for point torques (e.g., rotation of flagellar filament) and sources (e.g., growth of bubble) outside a stationary sphere. Since there are presumably more situations in which these solutions would be useful, in this article we derive and summarize these results and their derivations so that they can be easily accessed and extended if desired.

The paper is organised as follows. First we present our setup and notation in Sec. II. By linearity of the Stokes equations, a general rotlet may be decomposed into an axisymmetric and transverse component, which we then tackle in Secs. III and IV, respectively. Finally, the source is treated in Sec. V. In each case, we begin with the known preliminary result listed in Ref. [4] and then derive the solutions, first in the case of a rigid sphere (no-slip boundary condition) and next in the case of a spherical bubble (no-shear boundary condition). We complement our results with numerically obtained visualisations of the flow field in each case, and summarize our results in Sec. VI.

II. GEOMETRY AND SETUP

A. Geometry

The geometry of our problem is defined by a rigid sphere, or spherical bubble, centered at a point $\boldsymbol{x}_1$ (see sketch in Fig. 1). Whenever we refer to spherical coordinates $\{r, \theta, \phi\}$ in what follows, we define them with respect to the origin at $\boldsymbol{x}_1$. Since the radius of the sphere is the only extrinsic length scale in the problem, we choose to scale lengths such that the radius becomes unity. Without loss of generality, we can then consider a hydrodynamic singularity located at a point $\boldsymbol{x}_2$, where $\boldsymbol{x}_2 = \boldsymbol{x}_1 - R\boldsymbol{d}$, where $R > 1$ is the distance from the singularity to the sphere center and $\boldsymbol{d}$ a unit vector

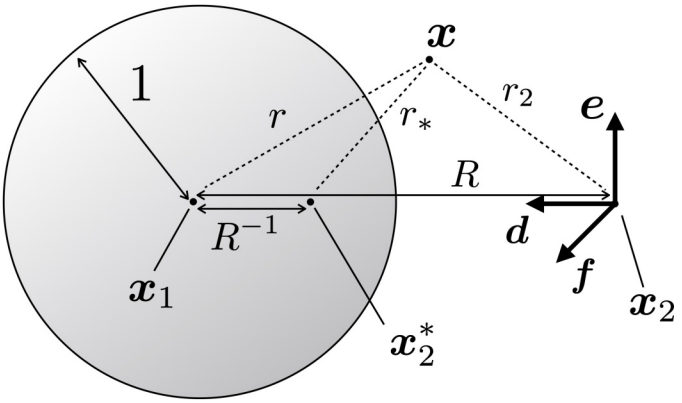

FIG. 1. Illustration of the geometrical setup for flow singularities in a spherical geometry. A Stokes flow is induced by hydrodynamic singularities placed at $\boldsymbol{x}_2$, a distance R from the center of a unit sphere positioned at $\boldsymbol{x}_1$. The mirror image point $\boldsymbol{x}_2^*$ is located a distance R^{-1} from $\boldsymbol{x}_1$ toward $\boldsymbol{x}_2$. The left-handed triad $\{\boldsymbol{d}, \boldsymbol{e}, \boldsymbol{f}\}$, and the lengths r, r_2, and r_* are defined in relation to $\boldsymbol{x}_1, \boldsymbol{x}_2, \boldsymbol{x}_2^*$ and a general point $\boldsymbol{x}$ as shown.

pointing from $\boldsymbol{x}_2$ to $\boldsymbol{x}_1$. To maintain a notation that is consistent with previous work [4,35,36] we extend this to a left-handed orthonormal triad $\{\boldsymbol{d}, \boldsymbol{e}, \boldsymbol{f}\}$. Furthermore, in what follows an important role will be played by the mirror image point $\boldsymbol{x}_2^*$, defined by $\boldsymbol{x}_2^* = \boldsymbol{x}_1 - R^{-1}\boldsymbol{d}$, and we will repeatedly refer to the distances defined by

$$r = |\boldsymbol{x} - \boldsymbol{x}_1|, \quad r_2 = |\boldsymbol{x} - \boldsymbol{x}_2|, \tag{1}$$

$$r_* = |\boldsymbol{x} - \boldsymbol{x}_2^*|, \quad \tilde{r}(\xi) = |\boldsymbol{x} + \xi \boldsymbol{d}|, \tag{2}$$

$$R = |\boldsymbol{x}_2 - \boldsymbol{x}_1|, \tag{3}$$

and the following shorthand,

$$D = \boldsymbol{d} \cdot \nabla = -\frac{\partial}{\partial r}, \tag{4}$$

for a gradient in the radial direction.

B. Problem setup

We consider the incompressible Stokes equations

$$\nabla p = \mu \nabla^2 \boldsymbol{u} + \boldsymbol{f}, \quad \nabla \cdot \boldsymbol{u} = 0, \tag{5}$$

where $\boldsymbol{u}$ is the fluid velocity field, p is dynamic pressure, μ is dynamic viscosity, and $\boldsymbol{f}$ a force density. In free space, the fundamental solution corresponds to a point force with $\boldsymbol{f}(\boldsymbol{x}) = \boldsymbol{F}\delta(\boldsymbol{x})$ and is given by

$$\boldsymbol{u}(\boldsymbol{x}) = \frac{\boldsymbol{F}}{8\pi\mu} \cdot \left(\frac{\boldsymbol{I}}{|\boldsymbol{x}|} + \frac{\boldsymbol{x}\boldsymbol{x}}{|\boldsymbol{x}|^3} \right) \equiv \boldsymbol{F} \cdot \boldsymbol{G}(\boldsymbol{x}), \quad p(\boldsymbol{x}) = \frac{\boldsymbol{F} \cdot \boldsymbol{x}}{4\pi |\boldsymbol{x}|^3}, \tag{6}$$

where $\boldsymbol{G}(\boldsymbol{x}) = (8\pi\mu|\boldsymbol{x}|^3)^{-1}(|\boldsymbol{x}|^2\boldsymbol{I} + \boldsymbol{x}\boldsymbol{x})$ is known as the Oseen tensor [4]. The solution in Eq. (6) is called the Stokeslet with strength $\boldsymbol{F}$.

The rotlet then emerges in the form of an antisymmetric force-dipole of the form $\frac{1}{2} g_a \varepsilon_{ajk} \nabla_k G_{ij}$ in index notation, where $\boldsymbol{g}$ is the rotlet strength and ε is the Levi-Civita tensor. The flow field may

be written in vector form as

$$\boldsymbol{u}(\boldsymbol{x}) = -\frac{1}{8\pi\mu}\boldsymbol{g}\times\nabla\frac{1}{|\boldsymbol{x}|} = \frac{1}{8\pi\mu}\frac{\boldsymbol{g}\times\boldsymbol{x}}{|\boldsymbol{x}|^3}, \quad p(\boldsymbol{x}) = 0. \tag{7}$$

Physically, a rotlet may be interpreted as the flow due to a point torque of strength $\boldsymbol{g}$ applied at the coordinate origin.

The solution for a point source cannot be directly obtained from the Green's function, since the latter is divergence-free while a point source is defined by the property that compressibility is locally singular. However, a simple mass conservation argument shows that a point source solution to Eq. (5) in free space is given by

$$\boldsymbol{u}(\boldsymbol{x}) = -\frac{Q}{4\pi}\nabla\frac{1}{|\boldsymbol{x}|} = \frac{Q}{4\pi|\boldsymbol{x}|^3}\boldsymbol{x}, \quad p(\boldsymbol{x}) = 0, \tag{8}$$

where Q has the interpretation of volume flux (with $Q > 0$ for a source and $Q < 0$ for a sink, respectively).

The goal of this article is to find the analog of Eq. (7) or Eq. (8) in the geometry described above. In the rigid-sphere case, we therefore seek the solution to Eq. (5) with boundary condition

$$\boldsymbol{u} = \boldsymbol{0} \quad \text{at} \quad r = 1, \tag{9a}$$

$$\boldsymbol{u} \to \boldsymbol{0} \quad \text{as} \quad r \to \infty. \tag{9b}$$

For a spherical bubble held in shape by surface tension γ (i.e., with vanishing Capillary number $\mathrm{Ca} = \mu U/\gamma$, where U is a characteristic scale for the flow velocity) the stress-free condition on the bubble surface leads to boundary conditions

$$\boldsymbol{n}\cdot\boldsymbol{u} = 0, \quad \boldsymbol{n}\times\boldsymbol{\sigma}\cdot\boldsymbol{n} = \boldsymbol{0} \quad \text{at} \quad r = 1, \tag{10a}$$

$$\boldsymbol{u} \to \boldsymbol{0} \quad \text{as} \quad r \to \infty, \tag{10b}$$

where $\boldsymbol{n} = \hat{\boldsymbol{r}}$ is defined as the unit normal to the sphere surface and $\boldsymbol{\sigma}$ is the hydrodynamic stress tensor, i.e., $\boldsymbol{\sigma} = -p\boldsymbol{I} + \mu(\nabla\boldsymbol{u} + (\nabla\boldsymbol{u})^T)$. Finally, we require that the solution diverges at $\boldsymbol{x}_2$ similarly to the divergence of $\boldsymbol{u}(\boldsymbol{x} - \boldsymbol{x}_2)$ in Eq. (7) or Eq. (8), i.e., that the difference between the solution and the free-space singularity remains bounded.

C. Method of solution

Fundamentally, in each case the solution may be written as

$$\boldsymbol{u} = \boldsymbol{u}_0 + \boldsymbol{u}_*, \tag{11}$$

where $\boldsymbol{u}_0$ is the flow due to the free-space singularities as in Eq. (7) or Eq. (8) and $\boldsymbol{u}_*$ is an image flow field that corrects for the boundary condition on the sphere surface and is therefore nonsingular everywhere in the fluid domain. In previous work [35,36] (see also the summary in Ref. [4]), $\boldsymbol{u}_*$ was derived for the Stokeslet by writing $\boldsymbol{u}_0$ in terms of spherical harmonics about $\boldsymbol{x}_1$, expanding the image system $\boldsymbol{u}_*$ as a multipole series about $\boldsymbol{x}_1$ also written in terms of spherical harmonics, and matching five infinite families of coefficients. The singularity solution is then obtained from the multipole expansion by postulating the equivalence to a line integral of finite-order singularities from $\boldsymbol{x}_1$ to $\boldsymbol{x}_2^*$ and again matching coefficients through the exploitation of a number of integral identities.

For the force dipole singularity, the literature only provides the multipole expansions of the image flow for (i) $(\boldsymbol{e}\cdot\nabla)\boldsymbol{d}\cdot\boldsymbol{G}(\boldsymbol{x} - \boldsymbol{x}_2)$, which is the difference between two axisymmetric Stokeslets with the difference taken in a line orthogonal to the line of centres, (ii) the image flow for $(\boldsymbol{d}\cdot\nabla)\boldsymbol{e}\cdot\boldsymbol{G}(\boldsymbol{x} - \boldsymbol{x}_2)$, which is the difference between two transverse Stokeslets with the difference taken in a line away from the sphere center, and (iii) the image flow for $(\boldsymbol{f}\cdot\nabla)\boldsymbol{e}\cdot\boldsymbol{G}(\boldsymbol{x} - \boldsymbol{x}_2)$, which is the

difference between two transverse Stokeslets with the difference taken in a line orthogonal to the line of centres and the line from the sphere center.

While the expressions for the singularity dipoles are equivalent up to a permutation of the vectors $\{\boldsymbol{d}, \boldsymbol{e}, \boldsymbol{f}\}$, the image flow depends on the direction in which gradients are taken, since the images all lie on the axis between $\boldsymbol{x}_1$ and $\boldsymbol{x}_2$, and perturbations in the $\boldsymbol{e}$-$\boldsymbol{f}$ plane change the direction of this axis. Despite the presence of some typographical errors in the derivations, we have verified the correctness of the relevant expressions given in Ref. [4] and take these as the starting point of our calculation for the rotlet. By linearity of the Stokes equations, a general rotlet may be decomposed into an axisymmetric (parallel to $\boldsymbol{d}$) and transverse (in the $\boldsymbol{e}$-$\boldsymbol{f}$ plane) component, so without loss of generality we tackle these separately in Secs. III and IV, respectively. For the source, we derive the solution from first principles in Sec. V.

III. THE AXISYMMETRIC ROTLET

A. No-slip boundary condition (rigid sphere)

1. Derivation

From the summary in Ref. [4] we quote the image for the dipole $(\boldsymbol{f}\cdot\boldsymbol{\nabla})\boldsymbol{e}\cdot\boldsymbol{G}(\boldsymbol{x}-\boldsymbol{x}_2)$, which can be written in terms of a multipole expansion as

$$\begin{aligned}\boldsymbol{u}_* = &\sum_{n=0}^{\infty}\frac{D^n}{n!}(A_n+B_n\nabla^2)(\boldsymbol{f}\cdot\boldsymbol{\nabla})\boldsymbol{e}\cdot\boldsymbol{G}(\boldsymbol{x}-\boldsymbol{x}_1)\\ &+\sum_{n=0}^{\infty}\frac{D^n}{8\pi\mu n!}[C_n(\boldsymbol{e}\times\boldsymbol{f})+C_{n+1}(\boldsymbol{f}\cdot\boldsymbol{\nabla})(\boldsymbol{e}\times\boldsymbol{d})]\times\boldsymbol{\nabla}r^{-1},\end{aligned} \tag{12}$$

where

$$A_n = \frac{n(2n+5)}{2(n+3)}R^{-(n+3)} - \frac{(n+2)(2n+3)}{2(n+3)}R^{-(n+5)}, \tag{13a}$$

$$B_n = \frac{n}{4(n+3)}R^{-(n+3)} - \frac{n^2+5n+3}{2(n+3)(n+5)}R^{-(n+5)} + \frac{n+2}{4(n+5)}R^{-(n+7)}, \tag{13b}$$

$$C_n = \frac{2n+3}{n+3}R^{-(n+3)} - \frac{2n+3}{n+3}R^{-(n+5)}. \tag{13c}$$

To obtain from this the image field of an axisymmetric dipole, we need to antisymmetrize this expression in the vectors $\boldsymbol{e}$ and $\boldsymbol{f}$. Defining $S_{jk} = (e_k f_j - e_j f_k)/2$ and noting that $\boldsymbol{e}\times\boldsymbol{f} = -\boldsymbol{d}$ we hence have the multipole expansion

$$[\boldsymbol{u}_*]_i = g\sum_{n=0}^{\infty}\frac{D^n}{n!}A_n S_{jk}\nabla_k G_{ij} + \frac{D^n}{8\pi\mu n!}[C_n d_a + C_{n+1}S_{jb}\nabla_b\varepsilon_{ajl}d_l]\varepsilon_{iak}\nabla_k r^{-1}, \tag{14}$$

for the image of an axisymmetric rotlet with $\boldsymbol{g} = g\boldsymbol{d}$. We note that the terms proportional to $\nabla^2\nabla_k G_{ij}$ have disappeared since they are symmetric in $\{i, j, k\}$. In addition we can exploit the identities $S_{jk}\nabla_k G_{ij} = 2S_{ik}\nabla_k r^{-1}$ and $2S_{jk} = d_a\varepsilon_{ajk}$ to simplify this result further and obtain an expression just in terms of derivatives of ∇r^{-1} as

$$[\boldsymbol{u}_*]_i = g\sum_{n=0}^{\infty}\frac{D^n}{8\pi\mu n!}\left[(C_n - A_n)d_a + \frac{1}{2}C_{n+1}\varepsilon_{ajl}\varepsilon_{cjb}d_c d_l\nabla_b\right]\varepsilon_{iak}\nabla_k r^{-1}. \tag{15}$$

Noting that $\boldsymbol{d}\cdot\boldsymbol{d}=1$ and $\nabla\times\nabla=\mathbf{0}$, this can be written more elegantly as

$$\boldsymbol{u}_*=\boldsymbol{g}\times\sum_{n=0}^{\infty}\frac{D^n}{8\pi\mu n!}\alpha_n\nabla r^{-1} \tag{16}$$

where

$$\alpha_n=\frac{n+2}{2}C_n-A_n=R^{-n-3}. \tag{17}$$

The goal of this calculation is then to replace the infinite sum of higher order singularities at the point $\boldsymbol{x}_1$ in Eq. (16) by a line integral of lower order singularities between $\boldsymbol{x}_1$ and $\boldsymbol{x}_2^*$. Specifically, we seek a solution of the form

$$\boldsymbol{u}_*=\frac{\boldsymbol{g}}{8\pi\mu}\times\int_0^{R^{-1}}f(\xi)\nabla\frac{1}{\tilde{r}}\,d\xi, \tag{18}$$

where $\tilde{r}=|\boldsymbol{x}-\boldsymbol{\xi}|$ and $\boldsymbol{\xi}=-\xi\boldsymbol{d}$. Here the upper limit of the integrals is to be understood as $R^{-1}+\varepsilon$ where $\varepsilon>0$ is infinitesimally small and f and g as identically zero for $\xi>R^{-1}$. As a consequence we have the identities

$$\int_0^{R^{-1}}\delta(\xi-R^{-1})\xi^n\,d\xi=R^{-n}, \tag{19}$$

$$\int_0^{R^{-1}}\delta'(\xi-R^{-1})\xi^n\,d\xi=-nR^{-(n-1)}, \tag{20}$$

$$\int_0^{R^{-1}}\xi^{k-1}\xi^n\,d\xi=\frac{R^{-(n+k)}}{n+k}. \tag{21}$$

These are useful when combined with the Taylor series of the singularities about $\boldsymbol{x}_1$,

$$\nabla\frac{1}{\tilde{r}}=\sum_{n=0}^{\infty}\xi^n\frac{D^n}{n!}\nabla\frac{1}{r}, \tag{22}$$

because this gives

$$\alpha_n=\int_0^{R^{-1}}f(\xi)\xi^n\,d\xi. \tag{23}$$

In this particular case, the relationship is straightforward and we have

$$f(\xi)=R^{-3}\delta(\xi-R^{-1}), \tag{24}$$

and so the flow is simply given by

$$\boldsymbol{u}=\frac{\boldsymbol{g}}{8\pi\mu}\times\left[-\nabla\frac{1}{r_2}+R^{-3}\nabla\frac{1}{r_*}\right], \tag{25}$$

where, as a reminder, the axisymmetric torque is defined by $\boldsymbol{g}=g\boldsymbol{d}$ and located at $\boldsymbol{x}_2$. It is straightforward to verify that this expression satisfies the boundary condition in Eq. (9).

2. Interpretation

Our results show that, similar to the case of a rigid wall [20], the image of the rotlet consists of just a single other rotlet, in this case with its strength modified by a factor of $-R^{-3}$. Since there is no Stokeslet response in the image, there is no net force exerted on the boundary in either case. However, the presence of a rotlet image response may be interpreted as due to a nonzero torque that

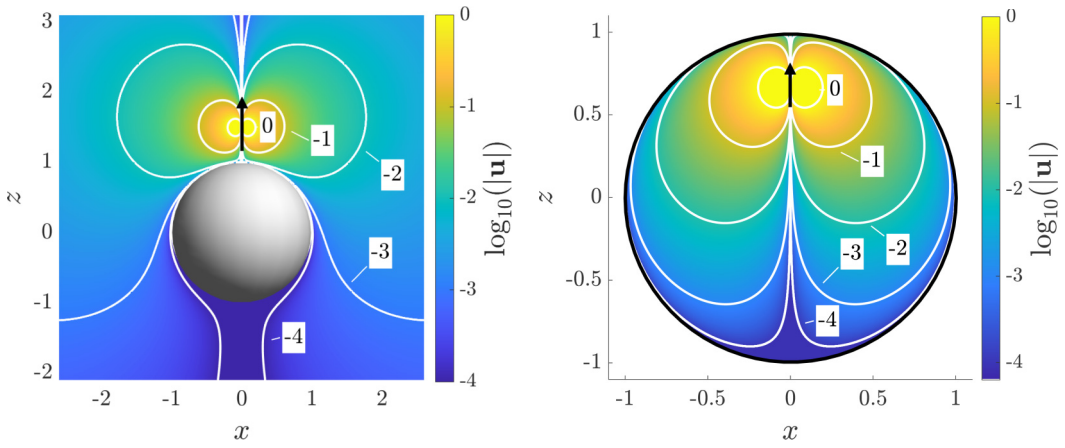

(a) Outside a rigid sphere

(b) Inside a spherical shell

FIG. 2. Logarithmic magnitude of the flow due to an axisymmetric rotlet in a Cartesian coordinate system with a rigid unit sphere at its origin and $\boldsymbol{g} = \hat{z}$. In (a) the rotlet is positioned outside the sphere at $\boldsymbol{x}_2 = \frac{3}{2}\hat{z}$, while in (b) it is located inside the sphere at $\boldsymbol{x}_2 = \frac{2}{3}\hat{z}$. At each point, the flow is directed azimuthally around the z axis. Bright yellow indicates regions of strong flow and dark blue regions of weak flow, while white contours are labeled with the order of magnitude of the flow. Black arrows indicate the position and orientation of the rotlet.

needs to be applied to the sphere to remain stationary. Indeed, the torque exerted by the rotlet on the sphere is given by

$$\boldsymbol{T}^{\text{rotlet, axisym}}_{\text{rigid}} = \alpha_0 \boldsymbol{g} = \frac{1}{R^3}\boldsymbol{g}. \tag{26}$$

An illustration of the flow field induced by the axisymmetric rotlet outside the sphere is shown in Fig. 2(a). We consider a rotlet with $\boldsymbol{g} = \boldsymbol{d}$ with $R = 3/2$ and use color to visualise the magnitude of the flow, with dark blue indicating weak and bright yellow indicating strong flow. The structure of the solution is reminiscent of the well known problem for the electrostatic potential due to a point charge outside a conducting sphere. In that case, the potential solves Laplace's equation, whose fundamental solution is proportional to $1/r_2$. This differs from the solution to the azimuthal component of the Stokes equations which is proportional to ρ/r_2^3. In both cases, however, the simplicity of the image system may be understood with the help of a geometric argument. Specifically, the image point $\boldsymbol{x}_2^*$ is defined in a way that the ratio r_*/r_2 is constant on the sphere surface, which may thus be interpreted as the surface of revolution of an Apollonian circle defined by $\boldsymbol{x}_2$ and $\boldsymbol{x}_2^*$. In the case of electrostatic charges, it is then immediate from this that the strength of the image charge may be chosen to meet an equipotential boundary condition on the sphere surface. In the case of the rotlet, this is only possible because ρ is the same for both the singularity and its image. However, we stress that the simple form of Eq. (25) is not to be expected *a priori* from the complexity of the image systems required to match the no-slip condition in many geometries. In fact, usually a free surface boundary condition leads to a simpler image system than a rigid boundary, though as we will show in Sec. III B this is not the case here.

A further implication of our results is that the equivalent solution for an axisymmetric rotlet inside a sphere ($R < 1$) may also be expressed by a single image singularity. The flow obtained in that case is illustrated in Fig. 2(b). The general case of an arbitrary rotlet inside a rigid spherical shell has been studied before using flow potentials [39,40], although this simple formulation for the axisymmetric case had not been identified.

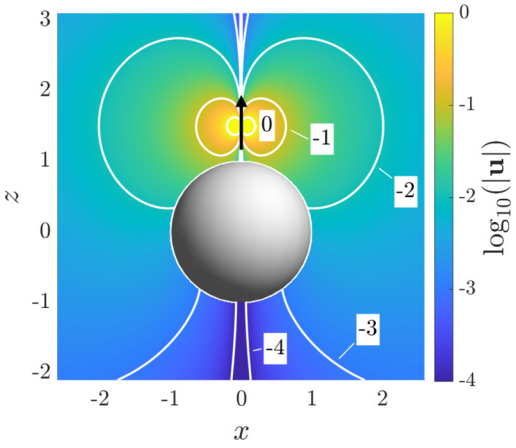

FIG. 3. Logarithmic magnitude of the flow due to an axisymmetric rotlet in a Cartesian coordinate system outside a spherical bubble at its origin, $\boldsymbol{g} = \hat{\boldsymbol{z}}$ and $\boldsymbol{x}_2 = \frac{3}{2}\hat{\boldsymbol{z}}$. At each point the flow is directed azimuthally around the z axis. Bright yellow indicates regions of strong flow and dark blue regions of weak flow, while white contours are labeled with the order of magnitude of the flow. A black arrow indicate the position and orientation of the rotlet.

B. No tangential stress boundary condition (spherical bubble)

To derive the solution for an axisymmetric rotlet outside a bubble, we follow a similar procedure to the one presented in Sec. III A. The structure of the solution is the same, but due to the different boundary conditions on the sphere surface, Eq. (10), the values of the coefficients A_n, B_n and C_n are different. Using expressions for the multipole expansions for Stokeslets outside a bubble listed in Ref. [4], it is possible to show that the dipole $(\boldsymbol{f}\cdot\nabla)\boldsymbol{e}\cdot\boldsymbol{G}(\boldsymbol{x}-\boldsymbol{x}_2)$ has the image

$$\boldsymbol{u}_* = \sum_{n=0}^{\infty} \frac{D^n}{n!} A_n (\boldsymbol{f}\cdot\nabla)\boldsymbol{e}\cdot\boldsymbol{G}(\boldsymbol{x}-\boldsymbol{x}_1), \tag{27}$$

where

$$A_n = \frac{n}{n+3} R^{-n-3}. \tag{28}$$

From this, it is straightforward to obtain

$$\alpha_n = -A_n = -R^{-3}R^{-n} + 3\frac{R^{-(n+3)}}{n+3}, \tag{29}$$

and following the same replacement rules as before we have

$$f(\xi) = -R^{-3}\delta(\xi - R^{-1}) + 3\xi^2. \tag{30}$$

The flow field due to an axisymmetric rotlet $\boldsymbol{g} = g\boldsymbol{d}$ outside a spherical bubble is therefore given by

$$\boldsymbol{u} = \frac{\boldsymbol{g}}{8\pi\mu}\times\left[-\nabla\frac{1}{r_2} - R^{-3}\nabla\frac{1}{r_*} + \int_0^{R^{-1}} 3\xi^2\nabla\frac{1}{\tilde{r}}\,d\xi\right], \tag{31}$$

corresponding to a point image rotlet and a line of image rotlets.

An illustration of the flow field obtained in this case is shown in Fig. 3. Surprisingly, its mathematical structure is more complex than in the case of a rigid boundary, which is unusual for boundary value problems in Stokes flow. Indeed, the much simpler form of the multipole expansion would suggest a simple image system, but this is not the case because of the substantial cancellation

that occurs in the rigid case. The simplicity of the earlier result is a nontrivial consequence of the geometry, boundary condition, and structure of the rotlet flow.

It may furthermore be verified that the bubble does not experience a torque due to the axisymmetric rotlet, as expected from the boundary condition of zero tangential stress, Eq. (10a). Indeed, the leading-order term in the multipole expansion, α_0, is equal to zero, and so

$$\boldsymbol{T}_{\text{bubble}}^{\text{rotlet, axisym}} = \boldsymbol{0}, \tag{32}$$

as required.

IV. THE TRANSVERSE ROTLET

A. No-slip boundary condition (rigid sphere)

1. Derivation

As might be expected from the broken symmetry, the relevant expressions for the case of a transverse rotlet, i.e., one such that $\boldsymbol{g}\cdot\boldsymbol{d}=0$, are more tedious. Once again we quote the image flow for the dipole $(\boldsymbol{e}\cdot\boldsymbol{\nabla})\boldsymbol{d}\cdot\boldsymbol{G}(\boldsymbol{x}-\boldsymbol{x}_2)$ from Ref. [4] as

$$\boldsymbol{u}_* = \sum_{n=0}^{\infty}\frac{D^n}{n!}\left[(\hat{A}_n+\hat{B}_n\nabla^2)\boldsymbol{e}\cdot\boldsymbol{G}(\boldsymbol{x}-\boldsymbol{x}_1)+\frac{\hat{C}_n}{8\pi\mu}\boldsymbol{f}\times\boldsymbol{\nabla}r^{-1}\right], \tag{33}$$

and for the dipole $(\boldsymbol{d}\cdot\boldsymbol{\nabla})\boldsymbol{e}\cdot\boldsymbol{G}(\boldsymbol{x}-\boldsymbol{x}_1)$ as

$$\boldsymbol{u}_* = \sum_{n=0}^{\infty}\frac{D^n}{n!}\left[(\tilde{A}_n+\tilde{B}_n\nabla^2)\boldsymbol{e}\cdot\boldsymbol{G}(\boldsymbol{x}-\boldsymbol{x}_2)+\frac{\tilde{C}_n}{8\pi\mu}\boldsymbol{f}\times\boldsymbol{\nabla}r^{-1}\right], \tag{34}$$

where the six families of coefficients are given by

$$\hat{A}_n = \frac{(2n^3+9n^2+10n+3)}{2(n+2)}R^{-(n+4)} - \frac{(2n^3+11n^2+14n+3)}{2(n+2)}R^{-(n+2)}, \tag{35a}$$

$$\tilde{A}_n = \frac{(2n^3+9n^2+10n+3)}{2(n+2)}R^{-(n+4)} - \frac{(2n^3+3n^2-2n-3)}{2(n+2)}R^{-(n+2)}, \tag{35b}$$

$$\hat{B}_n = -\frac{(n^2+6n+5)}{4(n+4)}R^{-(n+6)} + \frac{(n^3+8n^2+17n+7)}{2(n+2)(n+4)}R^{-(n+4)} - \frac{(n^2+4n+1)}{4(n+2)}R^{-(n+2)}, \tag{35c}$$

$$\tilde{B}_n = -\frac{(n^2+6n+5)}{4(n+4)}R^{-(n+6)} + \frac{(n^3+6n^2+8n-3)}{2(n+2)(n+4)}R^{-(n+4)} - \frac{(n^2-1)}{4(n+2)}R^{-(n+2)}, \tag{35d}$$

$$\hat{C}_n = \frac{(2n^2+11n+12)}{n+3}R^{-(n+5)} - \frac{(2n^2+13n+18)}{n+3}R^{-(n+3)}, \tag{35e}$$

$$\tilde{C}_n = \frac{(2n^2+11n+12)}{n+3}R^{-(n+5)} - \frac{(2n^2+7n+6)}{n+3}R^{-(n+3)}. \tag{35f}$$

For the antisymmetric dipole defined by $\frac{1}{2}g[(\boldsymbol{d}\cdot\boldsymbol{\nabla})\boldsymbol{e}-(\boldsymbol{e}\cdot\boldsymbol{\nabla})\boldsymbol{d}]\cdot\boldsymbol{G}$, corresponding to a rotlet with $\boldsymbol{g}=g\boldsymbol{f}$, we thus obtain that the image flow is given by

$$\boldsymbol{u}_* = g\sum_{n=0}^{\infty}\frac{D^n}{n!}\left[(\alpha_n+\beta_n\nabla^2)\boldsymbol{e}\cdot\boldsymbol{G}(\boldsymbol{x}-\boldsymbol{x}_1)+\frac{\gamma_n}{8\pi\mu}\boldsymbol{f}\times\boldsymbol{\nabla}r^{-1}\right], \tag{36}$$

where the coefficients simplify to

$$\alpha_n = \frac{1}{2}(\tilde{A}_n - \hat{A}_n) = 2R^{-3}nR^{-(n-1)} + \frac{3}{2}\frac{R^{-(n+2)}}{n+2}, \tag{37a}$$

$$\beta_n = \frac{1}{2}(\tilde{B}_n - \hat{B}_n) = -\frac{1}{2}(R^{-4} - R^{-2})R^{-n} - \frac{3}{4}\frac{R^{-(n+2)}}{n+2} + \frac{3}{4}\frac{R^{-(n+4)}}{n+4}, \tag{37b}$$

$$\gamma_n = \frac{1}{2}(\tilde{C}_n - \hat{C}_n) = 3R^{-3}R^{-n} - 3\frac{R^{-(n+3)}}{n+3}. \tag{37c}$$

In analogy with the axisymmetric case, we next want to write the solution as

$$\boldsymbol{u}_* = g\int_0^{R^{-1}} [f(\xi) + g(\xi)\nabla^2]\boldsymbol{e}\cdot\boldsymbol{G}(\boldsymbol{x}-\boldsymbol{\xi}) + \frac{h(\xi)}{8\pi\mu}\boldsymbol{f}\times\nabla\tilde{r}^{-1}\,d\xi, \tag{38}$$

which, in this case, requires that

$$\alpha_n = \int_0^{R^{-1}} f(\xi)\xi^n\,d\xi, \tag{39a}$$

$$\beta_n = \int_0^{R^{-1}} g(\xi)\xi^n\,d\xi, \tag{39b}$$

$$\gamma_n = \int_0^{R^{-1}} h(\xi)\xi^n\,d\xi. \tag{39c}$$

Thus, using again the identities in Eqs. (19)–(21), we find that

$$f(\xi) = -2R^{-3}\delta'(\xi - R^{-1}) + \tfrac{3}{2}\xi, \tag{40a}$$

$$g(\xi) = -\tfrac{1}{2}(R^{-4} - R^{-2})\delta(\xi - R^{-1}) - \tfrac{3}{4}(\xi - \xi^3), \tag{40b}$$

$$h(\xi) = 3R^{-3}\delta(\xi - R^{-1}) - 3\xi^2, \tag{40c}$$

and so

$$\begin{aligned}\boldsymbol{u}_* = g\Bigg\{&2R^{-3}D\boldsymbol{e}\cdot\boldsymbol{G}(\boldsymbol{x}-\boldsymbol{x}_2^*) - \frac{1}{2}(R^{-4}-R^{-2})\boldsymbol{e}\cdot\nabla^2\boldsymbol{G}(\boldsymbol{x}-\boldsymbol{x}_2^*) + \frac{3R^{-3}}{8\pi\mu}\boldsymbol{f}\times\nabla r_*^{-1}\\ &+\int_0^{R^{-1}}\left[\frac{3}{2}\xi - \frac{3}{4}(\xi-\xi^3)\nabla^2\right]\boldsymbol{e}\cdot\boldsymbol{G}(\boldsymbol{x}-\boldsymbol{\xi}) - \frac{3\xi^2}{8\pi\mu}\boldsymbol{f}\times\nabla\tilde{r}^{-1}\,d\xi\Bigg\}.\end{aligned} \tag{41}$$

Finally, we eliminate $\boldsymbol{e}$ by replacing it with $-\boldsymbol{f}\times\boldsymbol{d}$ to obtain an expression that is linear in the rotlet strength $\boldsymbol{g}$. For a general rotlet in the $\boldsymbol{e}$-$\boldsymbol{f}$ plane we can therefore write the flow field as

$$\begin{aligned}\boldsymbol{u} = &\frac{1}{8\pi\mu}\left[-\boldsymbol{g}\times\nabla\frac{1}{r_2} + 3R^{-3}\boldsymbol{g}\times\nabla\frac{1}{r_*}\right]\\ &+(\boldsymbol{g}\times\boldsymbol{d})\cdot\left[\frac{1}{2}(R^{-4}-R^{-2})\nabla^2 - 2R^{-3}(\boldsymbol{d}\cdot\nabla)\right]\boldsymbol{G}(\boldsymbol{x}-\boldsymbol{x}_2^*)\\ &-(\boldsymbol{g}\times\boldsymbol{d})\cdot\int_0^{R^{-1}}\left[\frac{3}{2}\xi - \frac{3}{4}(\xi-\xi^3)\nabla^2\right]\boldsymbol{G}(\boldsymbol{x}-\boldsymbol{\xi})\,d\xi\\ &-\frac{\boldsymbol{g}}{8\pi\mu}\times\int_0^{R^{-1}} 3\xi^2\nabla\frac{1}{\tilde{r}}\,d\xi.\end{aligned} \tag{42}$$

2. Interpretation

Evidently, the image system for the transverse rotlet is significantly more complicated than in the axisymmetric case. It is composed of three point singularities at $\boldsymbol{x}_2^*$, namely, a rotlet, a source dipole and a stresslet, as well as a line of three different singularities from $\boldsymbol{x}_1$ to $\boldsymbol{x}_2^*$: Stokeslets, source dipoles and rotlets. However, the integrals are nowhere singular and therefore can be readily evaluated by standard numerical routines.

Three representative illustrations of the flow field are given in Fig. 4. In contrast to the axisymmetric case, we observe two bifurcation points of the flow field as R is varied, occurring at $R \approx 2.71$ and $R = 3$. Between these a counterrotating vortex appears on the far side of the sphere, which is analysed in detail in Ref. [24] using a solution obtained with the use of flow potentials and sphere theorems. Interestingly, the far-field flow on the far side of the sphere is always in the direction opposite what is expected from a free rotlet. This is due to the Stokeslet response that appears in Eq. (42), which dominates over the original rotlet singularity due to its slower decay. Physically, this arises because a nonzero force needs to be exerted on the sphere to keep it stationary, and its slower decay dominates at long distances. The force and torque exerted by the rotlet on the sphere can be calculated from our solution. They are given by the coefficients α_0, α_1, and γ_0 in Eq. (37) as

$$\boldsymbol{F}^{\text{rotlet, transverse}}_{\text{rigid}} = \alpha_0 \boldsymbol{g} \times \boldsymbol{d} = \frac{3}{4R^2} \boldsymbol{g} \times \boldsymbol{d}, \tag{43}$$

$$\boldsymbol{T}^{\text{rotlet, transverse}}_{\text{rigid}} = (\gamma_0 - \alpha_1)\boldsymbol{g} = -\frac{1}{2R^3} \boldsymbol{g}, \tag{44}$$

both of which are consistent with the application of Faxén's law to a sphere in the background flow $\boldsymbol{u}_0$ [4].

B. No tangential stress boundary condition (spherical bubble)

In the case of a spherical bubble, we have a no-tangential-stress as well as a no-penetration boundary condition on the surface of the sphere, see Eq. (10). Using multipole expansions for the axisymmetric and transverse Stokeslet listed in Ref. [4], we obtain the image field for the dipole $(\boldsymbol{e} \cdot \nabla)\boldsymbol{d} \cdot \boldsymbol{G}(\boldsymbol{x} - \boldsymbol{x}_2)$ as

$$\boldsymbol{u}_* = \sum_{n=0}^{\infty} \frac{D^n}{n!} \left[\hat{A}_n \boldsymbol{e} \cdot \boldsymbol{G}(\boldsymbol{x} - \boldsymbol{x}_1) + \frac{\hat{C}_n}{8\pi\mu} \boldsymbol{f} \times \nabla \frac{1}{r} \right], \tag{45}$$

and the image field for the dipole $(\boldsymbol{d} \cdot \nabla)\boldsymbol{e} \cdot \boldsymbol{G}(\boldsymbol{x} - \boldsymbol{x}_2)$ as

$$\boldsymbol{u}_* = \sum_{n=0}^{\infty} \frac{D^n}{n!} \tilde{A}_n \boldsymbol{e} \cdot \boldsymbol{G}(\boldsymbol{x} - \boldsymbol{x}_1), \tag{46}$$

where

$$\hat{A}_n = -\frac{n^2 + 4n + 1}{n + 2} R^{-n-2}, \tag{47a}$$

$$\hat{C}_n = -2R^{-n-3}, \tag{47b}$$

$$\tilde{A}_n = -\frac{n^2 - 1}{n + 2} R^{-n-2}. \tag{47c}$$

In a familiar fashion we hence obtain the image for $\boldsymbol{g} = g\boldsymbol{f}$ as

$$\boldsymbol{u}_* = g \sum_{n=0}^{\infty} \frac{D^n}{n!} \left[\alpha_n \boldsymbol{e} \cdot \boldsymbol{G}(\boldsymbol{x} - \boldsymbol{x}_1) + \frac{\gamma_n}{8\pi\mu} \boldsymbol{f} \times \nabla r^{-1} \right], \tag{48}$$

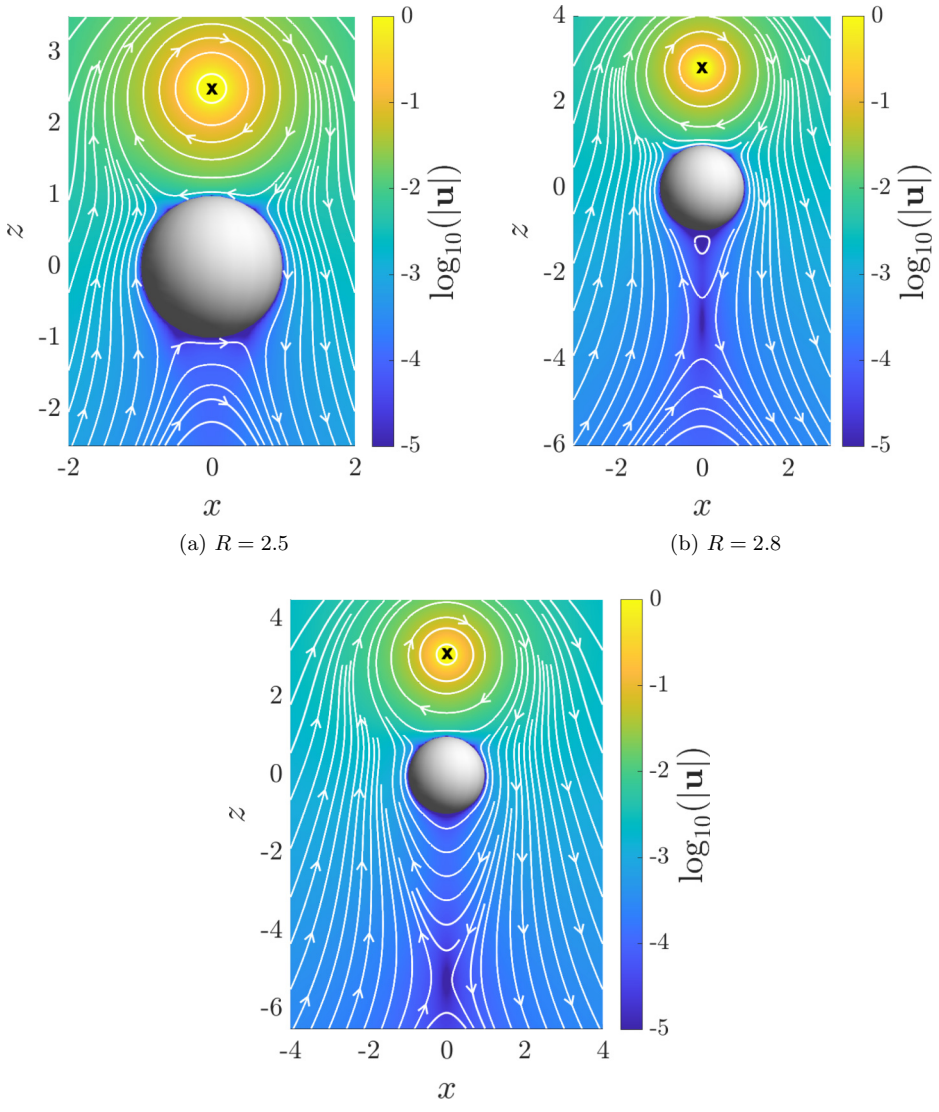

(a) $R = 2.5$ (b) $R = 2.8$

(c) $R = 3.1$

FIG. 4. Flow field in the x-z plane due to a transverse rotlet with $\boldsymbol{g} = \hat{\boldsymbol{y}}$ located at $\boldsymbol{x}_2 = R\hat{\boldsymbol{z}}$ outside a rigid unit sphere centered at the origin. Streamlines are drawn in white and the logarithm of the flow magnitude is superposed in color while black crosses indicate the position of the rotlet, pointing into the page. The flow undergoes two bifurcations as R increases, occurring at $R \approx 2.71$ and $R = 3$, between which a counterrotating vortex appears on the far side of the sphere.

where

$$\alpha_n = \frac{1}{2}(\tilde{A}_n - \hat{A}_n) = 2R^{-2}R^{-n} - 3\frac{R^{-(n+2)}}{n+2}, \tag{49a}$$

$$\gamma_n = -\frac{1}{2}\hat{C}_n = R^{-3}R^{-n}. \tag{49b}$$

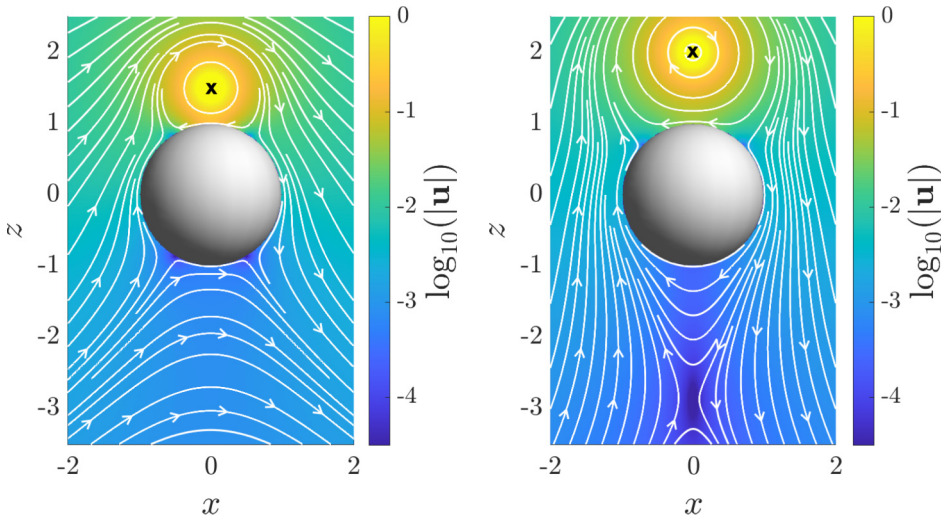

(a) $R = 1.5$ (b) $R = 2$

FIG. 5. Flow field in the x-z plane due to a transverse rotlet with $\boldsymbol{g} = \hat{\boldsymbol{y}}$ located at $\boldsymbol{x}_2 = R\hat{\boldsymbol{z}}$ outside a spherical bubble at the origin. Streamlines are drawn in white and the logarithm of the flow magnitude is superposed in color with black crosses indicating the position of the rotlet, pointing into the page. The flow undergoes one bifurcation at $R \approx 1.77$ as R increases where a saddle point appears on the far side of the sphere.

Using the same replacement rules as in Eqs. (19)–(21), we can write the flow due to a transverse rotlet outside a bubble as

$$\boldsymbol{u} = \frac{1}{8\pi\mu}\left[-\boldsymbol{g}\times\nabla\frac{1}{r_2} + R^{-3}\boldsymbol{g}\times\nabla\frac{1}{r_*}\right] - (\boldsymbol{g}\times\boldsymbol{d})\cdot 2R^{-2}\boldsymbol{G}(\boldsymbol{x}-\boldsymbol{x}_2^*) + (\boldsymbol{g}\times\boldsymbol{d})\cdot\int_0^{R^{-1}} 3\xi\boldsymbol{G}(\boldsymbol{x}-\boldsymbol{\xi})\,d\xi, \tag{50}$$

which may be interpreted as due to a point image rotlet, a point image Stokeslet and a line of Stokeslets.

An illustration of the flow is given in Fig. 5. In this case there is only a single bifurcation, which occurs as R increases to $R \approx 1.77$, where a saddle point appears on the far side of the bubble. Since the bubble surface cannot sustain any tangential stress, no counterrotating vortex emerges. Using the coefficients from Eq. (49a), the force and torque on the bubble are given by

$$\boldsymbol{F}^{\text{rotlet, transverse}}_{\text{bubble}} = \alpha_0\boldsymbol{g}\times\boldsymbol{d} = \frac{1}{2R^2}\boldsymbol{g}\times\boldsymbol{d}, \tag{51}$$

$$\boldsymbol{T}^{\text{rotlet, transverse}}_{\text{bubble}} = (\gamma_0 - \alpha_1)\boldsymbol{g} = \boldsymbol{0}, \tag{52}$$

where the latter was expected to be zero due to the no-stress boundary condition. This result is consistent with the generalisation of Faxén's law to a spherical bubble [41].

V. THE POINT SOURCE

A. The multipole expansion for a source

We now turn our attention to the problem involving a source (or sink). In this case there is no intermediate result that we can quote from the literature, and we need to start the derivation from

first principles. The flow due to a free space point source of strength Q located at $\boldsymbol{x}_2$ is

$$\boldsymbol{u}_0 = -\frac{Q}{4\pi}\boldsymbol{\nabla}\frac{1}{r_2} = \frac{Q}{4\pi r_2^3}\boldsymbol{r}_2. \tag{53}$$

Since $1/r$ is the fundamental solution to Laplace's equation, we can write $\boldsymbol{u}_0$ as a series of spherical harmonics about $\boldsymbol{x}_1$. Specifically, since we have the identity

$$\frac{D^n}{n!}\frac{1}{r} = \frac{P_n(-\boldsymbol{d}\cdot\hat{\boldsymbol{r}})}{r^{n+1}}, \tag{54}$$

where P_n is the nth Legendre polynomial, we can write

$$\frac{1}{r_2} = \sum_{n=0}^{\infty}\frac{r^{2n+1}}{R^{n+1}}\frac{D^n}{n!}\frac{1}{r}, \tag{55}$$

and therefore

$$\begin{aligned}\boldsymbol{u}_0 &= -\frac{Q}{4\pi}\boldsymbol{\nabla}\frac{1}{r_2} = \frac{Q}{4\pi}\sum_{n=0}^{\infty}-\boldsymbol{\nabla}\left[\frac{r^{2n+1}}{R^{n+1}}\frac{D^n}{n!}\frac{1}{r}\right]\\ &= \frac{Q}{4\pi}\sum_{n=0}^{\infty}\frac{r^{2n-1}}{R^{n+1}}[-(2n+1)(\boldsymbol{x}-\boldsymbol{x}_1) - r^2\boldsymbol{\nabla}]\frac{D^n}{n!}\frac{1}{r}.\end{aligned} \tag{56}$$

Furthermore, due to the axisymmetry of the flow field, the multipole expansion of the image field must take the form

$$\boldsymbol{u}_* = 2\mu Q\sum_{n=0}^{\infty}\frac{D^n}{n!}[A_n\boldsymbol{d}\cdot\boldsymbol{G}(\boldsymbol{x}-\boldsymbol{x}_1) + B_n\boldsymbol{d}\cdot\nabla^2\boldsymbol{G}(\boldsymbol{x}-\boldsymbol{x}_1)]. \tag{57}$$

In analogy with the work in Ref. [35], it may then be shown that

$$\boldsymbol{u}_* = \frac{Q}{4\pi}\sum_{n=1}^{\infty}\left\{-\frac{2(n+1)}{2n-1}A_{n-1}(\boldsymbol{x}-\boldsymbol{x}_1) + \left[\frac{(n-2)r^2}{2n-1}A_{n-1} - \frac{n}{2n+3}A_{n+1} - 2nB_{n-1}\right]\boldsymbol{\nabla}\right\}\frac{D^n}{n!}\frac{1}{r}. \tag{58}$$

Since the $n=0$ term in Eq. (59) is identically zero, we may write the total velocity $\boldsymbol{u} = \boldsymbol{u}_0 + \boldsymbol{u}_*$ as

$$\begin{aligned}\boldsymbol{u} = \frac{Q}{4\pi}\sum_{n=1}^{\infty}\Bigg\{&\left[-\frac{2(n+1)}{2n-1}A_{n-1} - \frac{(2n+1)r^{2n-1}}{R^{n+1}}\right](\boldsymbol{x}-\boldsymbol{x}_1)\\ &+\left[\frac{(n-2)r^2}{2n-1}A_{n-1} - \frac{n}{2n+3}A_{n+1} - 2nB_{n-1} - \frac{r^{2n+1}}{R^{n+1}}\right]\boldsymbol{\nabla}\Bigg\}\frac{D^n}{n!}\frac{1}{r}.\end{aligned} \tag{59}$$

To make further progress, we now distinguish between the problems of a source outside a rigid (no-slip) sphere, and outside a spherical no-shear bubble.

B. No-slip boundary condition (rigid sphere)

In this case the boundary condition is given by Eq. (9). By inspection, the condition on the surface of the sphere is equivalent to the two conditions

$$-\frac{2(n+1)}{2n-1}A_{n-1} - (2n+1)R^{-n-1} = 0, \tag{60a}$$

$$\frac{n-2}{2n-1}A_{n-1} - \frac{n}{2n+3}A_{n+1} - 2nB_{n-1} - R^{-n-1} = 0, \tag{60b}$$

whose solutions are

$$A_n = -\frac{(2n+1)(2n+3)}{2(n+2)}R^{-n-2} = 2R^{-3}(-nR^{-(n-1)}) - \frac{3}{2}\frac{R^{-n-2}}{n+2}, \tag{61a}$$

$$B_n = \frac{2n+7}{4(n+4)}R^{-n-4} - \frac{2n+1}{4(n+2)}R^{-n-2} = \frac{1}{2}(R^{-4}-R^{-2})R^{-n} + \frac{3}{4}\frac{R^{-n-2}}{n+2} - \frac{1}{4}\frac{R^{-n-4}}{n+4}. \tag{61b}$$

We can now follow the same procedure as for the rotlet in Sec. III A and convert this into a singularity solution of the form

$$\boldsymbol{u}_* = 2\mu Q\boldsymbol{d}\cdot\int_0^{R^{-1}}[f(\xi)+g(\xi)\nabla^2]\boldsymbol{G}(\boldsymbol{x}-\boldsymbol{\xi})\,d\xi, \tag{62}$$

which yields

$$f(\xi) = 2R^{-3}\delta'(\xi-R^{-1}) - \tfrac{3}{2}\xi, \tag{63a}$$

$$g(\xi) = \tfrac{1}{2}(R^{-4}-R^{-2})\delta(\xi-R^{-1}) + \frac{1}{4}(3\xi-\xi^3), \tag{63b}$$

and hence

$$\begin{aligned}\boldsymbol{u} = &-\frac{Q}{4\pi}\nabla\frac{1}{r_2} + 2\mu Q\boldsymbol{d}\cdot\left\{-2R^{-3}(\boldsymbol{d}\cdot\nabla)\boldsymbol{G}(\boldsymbol{x}-\boldsymbol{x}_2^*) + \frac{1}{2}(R^{-4}-R^{-2})\cdot\nabla^2\boldsymbol{G}(\boldsymbol{x}-\boldsymbol{x}_2^*)\right.\\ &\left.+\int_0^{R^{-1}}\left[-\frac{3}{2}\xi+\frac{1}{4}(3\xi-\xi^3)\nabla^2\right]\boldsymbol{G}(\boldsymbol{x}-\boldsymbol{\xi})\,d\xi\right\}.\end{aligned} \tag{64}$$

The image field for the source is therefore due to a point stresslet and point source dipole, as well as a line of Stokeslets and source dipoles. Note that, as expected from mass conservation across the sphere surface, it does not contain another source term. Furthermore, even though the axisymmetric source dipole only requires a finite number of images [35], this is not the case for a source.

Since a distribution of Stokeslets is present on the line between $\boldsymbol{x}_1$ and $\boldsymbol{x}_2$, the net force on the sphere due to the source is nonzero. That force is given by the zeroth term in the Stokeslet multipole expansion, A_0, which leads to

$$\boldsymbol{F}^{\text{source}}_{\text{rigid}} = -2\mu Q A_0\boldsymbol{d} = \frac{3\mu Q}{2R^2}\boldsymbol{d}, \tag{65}$$

which once again is consistent with Faxén's law [4]. By axisymmetry, the torque on the sphere vanishes.

An illustration of the flow field is shown in Fig. 6. This time there are three qualitative bifurcations in the flow features as R is increased from 1. The first is a saddle-node bifurcation at $R \approx 4.82$, which gives rise to a vortex ring in the wake of the sphere. A further transition at $R \approx 4.99$ changes the structure of the vortex, and it disappears again at $R \approx 5.81$.

C. No tangential stress boundary condition (spherical bubble)

In the case of a bubble we have a no-penetration velocity boundary condition, as well as the requirement of vanishing tangential stress on the sphere surface, Eq. (10). The condition that the normal velocity vanishes may be obtained by taking the $\hat{\boldsymbol{r}}$ component of Eq. (59). Noting from Eq. (54) that $D^n(r^{-1})/n! \sim r^{-n-1}$ we have the result

$$-\frac{n(n+1)}{2n-1}A_{n-1} + \frac{n(n+1)}{2n+3}A_{n+1} + 2n(n+1)B_{n-1} - nR^{-n-1} = 0. \tag{66}$$

For the tangential stress condition, we observe that since the flow is axisymmetric the boundary condition simply requires that the component $\sigma_{r\theta}$ of the stress tensor vanishes on the sphere surface.

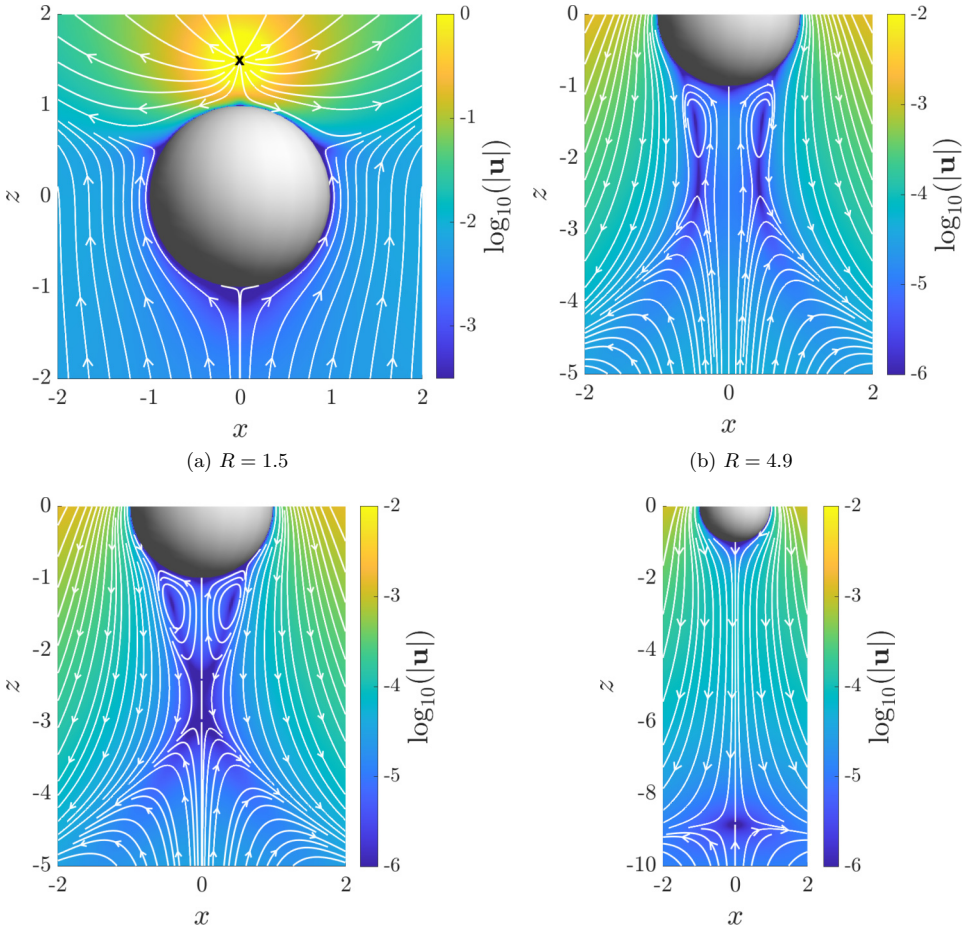

(a) $R = 1.5$ (b) $R = 4.9$

(c) $R = 5$ (d) $R = 5.85$

FIG. 6. Flow field in the x-z plane due to a source with $Q = 1$ located at $\boldsymbol{x}_2 = R\hat{\boldsymbol{z}}$ outside a rigid sphere at the origin. Streamlines are drawn in white and the logarithm of the flow magnitude is superposed in color. The black cross indicates the position of the source. The flow undergoes three bifurcations as R increases, at $R \approx 4.82$, $R \approx 4.99$, and $R \approx 5.81$, with a vortex ring appearing in the wake of the sphere at intermediate values of R.

In spherical polar coordinates about $\boldsymbol{x}_1$ this stress component is given by

$$\sigma_{r\theta} = \mu\left[r\frac{\partial}{\partial r}\left(\frac{u_\theta}{r}\right) + \frac{1}{r}\frac{\partial u_r}{\partial \theta}\right], \tag{67}$$

but since u_r is zero at $r = 1$ for all values of θ, the no-stress boundary condition becomes just

$$\left.\frac{\partial}{\partial r}\left(\frac{u_\theta}{r}\right)\right|_{r=1} = 0. \tag{68}$$

Defining the projection operator $\boldsymbol{\Pi} = \boldsymbol{I} - \hat{\boldsymbol{r}}\hat{\boldsymbol{r}}$, it is easy to see from Eq. (54) that $\boldsymbol{\Pi} \cdot \boldsymbol{\nabla} D^n(r^{-1})/n! \sim r^{-n-2}$ and thus Eq. (68) reduces to

$$-\frac{(n+1)(n-2)}{2n-1}A_{n-1} + \frac{n(n+3)}{2n+3}A_{n+1} + 2n(n+3)B_{n-1} - (n-2)R^{-n-1} = 0. \tag{69}$$

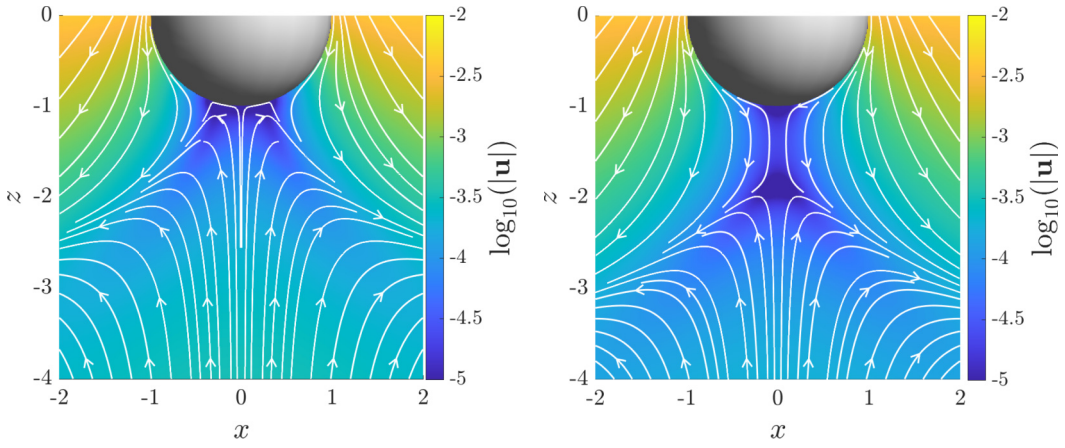

(a) $R = 2.9$ (b) $R = 3.1$

FIG. 7. Flow field in the x-z plane due to a source with $Q = 1$ located at $\boldsymbol{x}_2 = R\hat{\boldsymbol{z}}$ outside a spherical bubble at the origin. Streamlines are drawn in white and the logarithm of the flow magnitude is superposed in color. The flow undergoes one bifurcation at $R = 3$.

The system given by Eqs. (66) and (69) may then be solved to give

$$A_n = -2R^{-2}R^{-n} + 3\frac{R^{-(n+2)}}{n+2}, \tag{70a}$$

$$B_n = \frac{1}{2}\frac{R^{-(n+4)}}{n+4}, \tag{70b}$$

which lead to the flow field

$$\boldsymbol{u} = -\frac{Q}{4\pi}\boldsymbol{\nabla}\frac{1}{r_2} + 2\mu Q\boldsymbol{d}\cdot\left[-2R^{-2}\boldsymbol{G}(\boldsymbol{x}-\boldsymbol{x}_2^*) + \int_0^{R^{-1}}\left(3\xi + \frac{1}{2}\xi^3\nabla^2\right)\boldsymbol{G}(\boldsymbol{x}-\boldsymbol{\xi})\,d\xi\right]. \tag{71}$$

The image field for a point source outside a bubble may therefore be represented by a point Stokeslet, together with a line of Stokeslets and source dipoles. An illustration of this flow is shown in Fig. 7. Only one bifurcation of the flow field occurs, at $R = 1$. As in the case of the rotlet, the zero-shear condition on the bubble surface prevents the formation of a vortex in the bubble wake.

By considering the coefficient A_0, we obtain that the force on the bubble is

$$\boldsymbol{F}^{\text{source}}_{\text{bubble}} = \frac{\mu Q}{R^2}\boldsymbol{d} = \frac{1}{6}\boldsymbol{F}^{\text{source}}_{\text{rigid}}, \tag{72}$$

and its value is six times smaller than the force on a rigid sphere. The torque is zero again, as required for a bubble.

VI. DISCUSSION

In this article we derived physically-intuitive expressions for the flow due to an arbitrary point torque (rotlet, split into axisymmetric and transverse components) and a point source exterior to either a rigid sphere or a spherical bubble in Stokes flow. In the case of an axisymmetric rotlet outside a rigid sphere, the image flow may be interpreted as due to a single image torque, which can be explained using an argument involving Apollonian circles. The solution is therefore equally valid for an axisymmetric torque inside a spherical shell. Surprisingly, we find that the image field is much simpler in the rigid case than for a bubble, contrary to the other situations considered in this article and most known singularity solutions near plane surfaces [22]. In the transverse rotlet case,

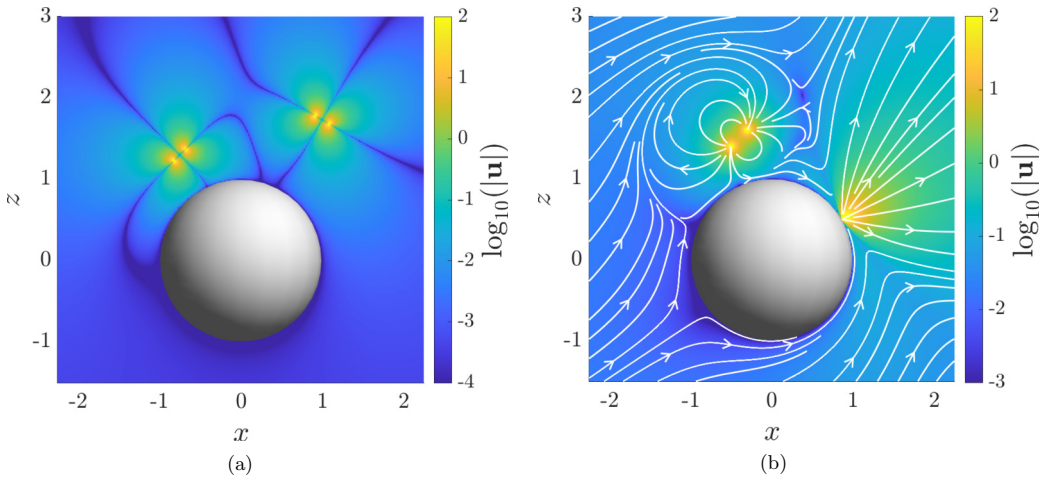

FIG. 8. Illustration of two systems that can be modeled using a superposition of hydrodynamic singularities derived in this paper (flow magnitudes shown on a logarithmic scale). (a) Interaction between two rotlet-dipoles near a rigid sphere, as relevant for the locomotion of helically flagellated bacteria. (b) A source-dipole microswimmer, modeling a self-diffusiophoretic Janus particle, near a rigid sphere emitting fluid at one location on its surface.

the image system is more complicated and involves multiple line integrals of singularities, yet the expression remains compact and easy to evaluate numerically. Two bifurcations occur in the flow field as the distance of the singularity to the sphere center varies. In the case of a point source, the solution cannot be written in terms of a finite number of images for either a rigid or a stress-free (bubble) boundary condition.

In addition to classical applications for the hydrodynamic interactions between colloidal particles [6], our results could be useful for the theoretical modeling of biologically motivated hydrodynamic problems, such as the interaction of rotating bacterial flagella with the cell body [37,42,43]. Our results are easily implemented and calculated numerically, and particularly suited to modeling the interaction of any number of singularities in an object-oriented programming style. The result for an axisymmetric torque within a rigid spherical shell may find additional use in the modeling of flows transport within biological cells [40,44]. Furthermore, closely separated singularities can be used to model dipoles, which appear in the flow signature of swimming bacteria [22] and artificial colloids [45]. A proof-of-concept illustration is shown in Fig. 8 in the case of two rotlet-dipoles near a rigid sphere (as relevant for the locomotion of helically flagellated bacteria) and a source-dipole (modeling a Janus colloid swimming via self-diffusiophoresis) near a rigid sphere that also emits fluid at one location on its surface.

Recently, regularized hydrodynamic singularities [46,47] have become a popular tool to carry out efficient numerical simulations of the dynamics slender filaments in Stokes flow [48–50] and great progress has been made in employing them to reduce numerical stiffness [33,51]. Regularizing a singularity in a nontrivial geometry also requires a modification of its image flow field to preserve the boundary condition, and doing this turns out to not be straightforward [31]. While this has been achieved for the Stokeslet [52], more work needs to be done to derive regularized versions of the rotlet and the source in a spherical geometry. We hope that the work outlined in this article will be useful for this purpose, too.

ACKNOWLEDGMENTS

The authors thank John Lister for helpful discussions and bringing Ref. [41] to our attention. This project has received funding from the European Research Council (ERC) under the European Union's Horizon 2020 research and innovation programme (Grant Agreement No. 682754 to E.L.).

[1] G. G. Stokes, *On the Effect of the Internal Friction of Fluids on the Motion of Pendulums*, Vol. 9 (Pitt Press, Cambridge, 1851).
[2] C. W. Oseen, Neuere Methoden und Ergebnisse in der Hydrodynamik, *Leipzig: Akademische Verlagsgesellschaft mb H.* (1927).
[3] J. Happel and H. Brenner, *Low Reynolds Number Hydrodynamics: With Special Applications to Particulate Media*, Vol. 1 (Springer Science & Business Media, Berlin, 2012).
[4] S. Kim and S. J. Karrila, *Microhydrodynamics: Principles and Selected Applications* (Courier Corporation, North Chelmsford, MA, 2013).
[5] H. Ockendon and J. R. Ockendon, *Viscous Flow*, Vol. 13 (Cambridge University Press, Cambridge, UK, 1995).
[6] E. Guazzelli and J. F. Morris, *A Physical Introduction to Suspension Dynamics*, Vol. 45 (Cambridge University Press, Cambridge, UK, 2011).
[7] H. A. Lorentz, Eene algemeene stelling omtrent de beweging eener vloeistof met wrijving en eenige daaruit afgeleide gevolgen, Zittingsverlag Akad. Wet. Amsterdam **5**, 168 (1896).
[8] G. Batchelor, The stress system in a suspension of force-free particles, J. Fluid Mech. **41**, 545 (1970).
[9] D. Saintillan and M. J. Shelley, Instabilities, pattern formation, and mixing in active suspensions, Phys. Fluids **20**, 123304 (2008).
[10] D. Saintillan, Rheology of active fluids, Annu. Rev. Fluid Mech. **50**, 563 (2018).
[11] D. Bray, *Cell Movements: From Molecules to Motility* (Garland Science, New York, NY, 2000).
[12] J. Lighthill, *Mathematical biofluiddynamics* (SIAM, Philadelphia, PA, 1975).
[13] T. Wu, C. J. Brokaw, and C. Brennen, *Swimming and Flying in Nature* Vol. 2 (Springer, Berlin, 1975).
[14] A. P. Berke, L. Turner, H. C. Berg, and E. Lauga, Hydrodynamic Attraction of Swimming Microorganisms by Surfaces, Phys. Rev. Lett. **101**, 038102 (2008).
[15] E. Lauga and T. R. Powers, The hydrodynamics of swimming microorganisms, Rep. Prog. Phys. **72**, 096601 (2009).
[16] K. Drescher, J. Dunkel, L. H. Cisneros, S. Ganguly, and R. E. Goldstein, Fluid dynamics and noise in bacterial cell–cell and cell–surface scattering, Proc. Natl. Acad. Sci. USA **108**, 10940 (2011).
[17] E. Lauga, Bacterial hydrodynamics, Annu. Rev. Fluid Mech. **48**, 105 (2016).
[18] C. Pozrikidis *et al.*, *Boundary Integral and Singularity Methods for Linearized Viscous Flow* (Cambridge University Press, Cambridge, UK, 1992).
[19] J. Blake, A note on the image system for a Stokeslet in a no-slip boundary, in *Mathematical Proceedings of the Cambridge Philosophical Society*, Vol. 70 (Cambridge University Press, Cambridge, UK, 1971), pp. 303–310.
[20] J. Blake and A. Chwang, Fundamental singularities of viscous flow, J. Eng. Math. **8**, 23 (1974).
[21] A. T. Chwang and T. Y.-T. Wu, Hydromechanics of low-Reynolds-number flow. Part 2. Singularity method for Stokes flows, J. Fluid Mech. **67**, 787 (1975).
[22] S. E. Spagnolie and E. Lauga, Hydrodynamics of self-propulsion near a boundary: Predictions and accuracy of far-field approximations, J. Fluid Mech. **700**, 105 (2012).
[23] K. Aderogba and J. Blake, Action of a force near the planar surface between two semi-infinite immiscible liquids at very low Reynolds numbers, Bull. Australian Math. Soc. **18**, 345 (1978).
[24] R. Shail and S. Onslow, Some Stokes flows exterior to a spherical boundary, Mathematika **35**, 233 (1988).
[25] S. Butler, A note on Stokes's stream function for motion with a spherical boundary, in *Mathematical Proceedings of the Cambridge Philosophical Society*, Vol. 49 (Cambridge University Press, Cambridge, UK, 1953), pp. 169–174.
[26] R. Shail, A note on some asymmetric Stokes flows within a sphere, Quart. J. Mech. Appl. Math. **40**, 223 (1987).
[27] C. Maul and S. Kim, Image systems for a Stokeslet inside a rigid spherical container, Phys. Fluids **6**, 2221 (1994).
[28] N. Liron and S. Mochon, Stokes flow for a Stokeslet between two parallel flat plates, J. Eng. Math. **10**, 287 (1976).
[29] V. Škultéty and A. Morozov, A note on forces exerted by a Stokeslet on confining boundaries, J. Fluid Mech. **882**, A1 (2020).

[30] R. Cortez, The method of regularized Stokeslets, SIAM J. Sci. Comput. **23**, 1204 (2001).
[31] J. Ainley, S. Durkin, R. Embid, P. Boindala, and R. Cortez, The method of images for regularized Stokeslets, J. Comput. Phys. **227**, 4600 (2008).
[32] R. Cortez and D. Varela, A general system of images for regularized Stokeslets and other elements near a plane wall, J. Comput. Phys. **285**, 41 (2015).
[33] A. L. Hall-McNair, T. D. Montenegro-Johnson, H. Gadêlha, D. J. Smith, and M. T. Gallagher, Efficient implementation of elastohydrodynamics via integral operators, Phys. Rev. Fluids **4**, 113101 (2019).
[34] H. Lamb, *Hydrodynamics* (Cambridge University Press, Cambridge, UK, 1993).
[35] Y. O. Fuentes, S. Kim, and D. J. Jeffrey, Mobility functions for two unequal viscous drops in Stokes flow. i. axisymmetric motions, Phys. Fluids **31**, 2445 (1988).
[36] Y. O. Fuentes, S. Kim, and D. J. Jeffrey, Mobility functions for two unequal viscous drops in Stokes flow. II. Asymmetric motions, Phys. Fluids A: Fluid Dynam. **1**, 61 (1989).
[37] A. Chamolly and E. Lauga, Direct vs indirect hydrodynamic interactions during bundle formation of bacterial flagella (unpublished).
[38] G. Gallino, F. Gallaire, E. Lauga, and S. Michelin, Physics of bubble-propelled microrockets, Adv. Funct. Mater. **28**, 1800686 (2018).
[39] W. Hackborn, M. O'Neill, and K. Ranger, The structure of an asymmetric Stokes flow, Quart. J. Mech. Appl. Math. **39**, 1 (1986).
[40] Y. Hernández-Pereira, A. O. Guerrero, J. M. Rendón-Mancha, and I. Tuval, On the necessary conditions for nonequivalent solutions of the rotlet-induced Stokes flow in a sphere: Towards a minimal model for fluid flow in the Kupffer's vesicle, Mathematics **8**, 1 (2020).
[41] J. Rallison, Note on the Faxén relations for a particle in Stokes flow, J. Fluid Mech. **88**, 529 (1978).
[42] T. R. Powers, Role of body rotation in bacterial flagellar bundling, Phys. Rev. E **65**, 040903(R) (2002).
[43] H. Flores, E. Lobaton, S. Mendez-Diez, S. Tlupova, and R. Cortez, A study of bacterial flagellar bundling, Bulletin Math. Biol. **67**, 137 (2005).
[44] D. Needleman and M. Shelley, The stormy fluid dynamics of the living cell, Phys. Today **72**, 32 (2019).
[45] T. Bickel, A. Majee, and A. Würger, Flow pattern in the vicinity of self-propelling hot Janus particles, Phys. Rev. E **88**, 012301 (2013).
[46] R. Cortez, L. Fauci, and A. Medovikov, The method of regularized Stokeslets in three dimensions: Analysis, validation, and application to helical swimming, Phys. Fluids **17**, 031504 (2005).
[47] B. Zhao, E. Lauga, and L. Koens, Method of regularized Stokeslets: Flow analysis and improvement of convergence, Phys. Rev. Fluids **4**, 084104 (2019).
[48] D. J. Smith, A boundary element regularized Stokeslet method applied to cilia-and flagella-driven flow, Proc. Roy. Soc. A: Math., Phys. Eng. Sci. **465**, 3605 (2009).
[49] T. D. Montenegro-Johnson, L. Koens, and E. Lauga, Microscale flow dynamics of ribbons and sheets, Soft Matter **13**, 546 (2017).
[50] K. Ishimoto and E. A. Gaffney, An elastohydrodynamical simulation study of filament and spermatozoan swimming driven by internal couples, IMA J. Appl. Math. **83**, 655 (2018).
[51] R. Cortez, Regularized Stokeslet segments, J. Comput. Phys. **375**, 783 (2018).
[52] J. K. Wróbel, R. Cortez, D. Varela, and L. Fauci, Regularized image system for Stokes flow outside a solid sphere, J. Comput. Phys. **317**, 165 (2016).